High Efficiency Quantum Dot Heterojunction Solar Cell Using Anatase (001) TiO_2 Nanosheets

Lioz Etgar, Wei Zhang, Stefanie Gabriel, Stephen G. Hickey, Md K. Nazeeruddin, Alexander Eychmüller, Bin Liu, and Michael Grätzel*

Quantum dots (QDs) have attracted a lot of attention due to their tunable bandgap and their high optical absorption cross section.[1–3] A variety of research projects attempt to integrate QDs into solar cells devices, including nanocrystal (NC)-polymer hybrid solar cells, NC-Schottky solar cells, NC-sensitized titanium dioxide (TiO_2) solar cells, and NC hybrid bilayer solar cells.[4–12] Recently investigations focus on QD heterojunction solar cells, by placing oxide NCs (TiO_2 or ZnO) as a thin spacer layer between the QDs and the FTO.[13–19] In addition, a tandem QD solar cell with the same structure has been demonstrated as well.[20] Multiple exciton generation (MEG) effect was also demonstrate in similar QD based solar cell structure.[21]

PbS and PbSe QDs belong to group IV-VI, which are known for their high absorbance in the visible and in the near infrared regions. They have a relatively large Bohr radius,[22–24] large ground state cross section of absorption (~10–15 cm^{-2}) and long excitonic lifetime (~200–800 ns).[25] In addition their bandgap can be tuned between 0.3–2.0 eV

The crystal structure of anatase TiO_2 can be theoretically constructed as truncated octahedron with eight equivalent (101) facets and two equivalent (001) facets on the top/bottom.[26] Studies have shown that the (001) facets of anatase TiO_2 are more reactive than the (101) facets which are more thermodynamically stable.[27] Moreover, the band edge of anatase TiO_2 with dominant (101) facets is more negative than the exposed (001) anatase TiO_2.[28]

Here we report on a QD heterojunction solar cell using anatase TiO_2 nanosheets with dominant (001) facets as photoanode. The anatase (001) TiO_2 nanosheets were synthesized via a simple hydrothermal route using tetrabutyl titanate, as the precursor and hydrofluoric acid solution as the solvent. Two sizes of nanosheets were synthesized with rectangular sheet-like structures, small nanosheets with a side length of ~30 nm and a thickness of ~7 nm, and big nanosheets consist of a side length of 60–80 nm and a thickness of ~8 nm. The PbS QDs in this heterojunction solar cell act as an absorber and at the same time as a hole conductor, rendering superfluous the use of an additional p-type material for transporting positive charge carriers. This simple PbS QD/TiO_2 nanosheets heterojunction solar cell achieved a remarkable short circuit current density (*J*sc) of 20.5 mA cm^{-2} and a light to electric power conversion efficiency (PCE) of 4.73% under 0.9 sun intensity. This is the first report of using anatase TiO_2 nanosheets with exposed (001) facets in a QD heterojunction solar cell.

TiO_2 nanosheets were synthesized via a simple hydrothermal route using tetrabutyl titanate, $Ti(OBu)_4$, as the precursor and 47% hydrofluoric acid solution as the solvent (see the experimental section for details). **Figure 1**A shows a typical X-ray diffraction (XRD) pattern of TiO_2 nanosheets synthesized at 180 and 200 °C. All the diffraction peaks are indexed to the anatase phase of TiO_2 (JCPDS No. 21-1272), indicating that the obtained product was pure anatase TiO_2 nanosheets. Figure 1B shows a high-magnification TEM image of an individual TiO_2 nanosheet. The lattice spacing parallel to the top and bottom facets was determined to be 0.235 nm, corresponding to the (001) planes of anatase TiO_2. The corresponding selected-area electron diffraction (SAED) pattern (indexed as the [001] zone axis diffraction) as shown in the inset of Figure 1A further indicates that the top and bottom facets of the nanosheets are the (001) planes. The low-magnification transmission electron microscopy (TEM) images of the obtained small and large TiO_2 nanosheets are shown in Figures 1C and 1D, respectively. The small nanosheets consist of well-defined rectangular sheet-like structures with a side length of 30 nm and a thickness of 7 nm, while the big nanosheets consist of well-defined rectangular sheet-like structures with a side length of 60–80 nm and a thickness of 8 nm.

On the basis of the above structural information, the percentage of highly reactive (001) facets in the small TiO_2 nanosheets (30 nm) was estimated to be 65% and the percentage of highly reactive (001) facets in the big TiO_2 nanosheets (80 nm) was estimated to be 75%. In addition, from BET analysis, the surface areas of the small and big TiO_2 nanosheets are determined to be 122 and 72 m^2/g, respectively.

The prepared TiO_2 nanosheets were used for the fabrication of heterojunction PbS QD/TiO_2 solar cells. **Figures 2**A and 2B present a scheme of the device structure. The bottom layer is composed of compact TiO_2 and TiO_2 nanosheets with exposed (001) facets layers acting as electron collectors. The light is absorbed by PbS QD film, which was made using layer-by-layer deposition technique. The original ligands of the PbS QDs

Dr. L. Etgar, Dr. Md. K. Nazeeruddin, Prof. M. Grätzel
Department of Sciences and Chemical Engineering
École Polytechnique Fédérale de Lausanne- EPFL
Lausanne, Switzerland
E-mail: lioz.etgar@epfl.ch
Mr. W. Zhang, Prof. B. Liu
Department of Chemical and Biomolecular Engineering
National university of Singapore, Singapore
S. Gabriel, Dr. S. G. Hickey, Prof. A. Eychmüller
Department of Physical Chemistry/Electrochemistry
TU Dresden, Dresden, Germany

DOI: 10.1002/adma.201104497

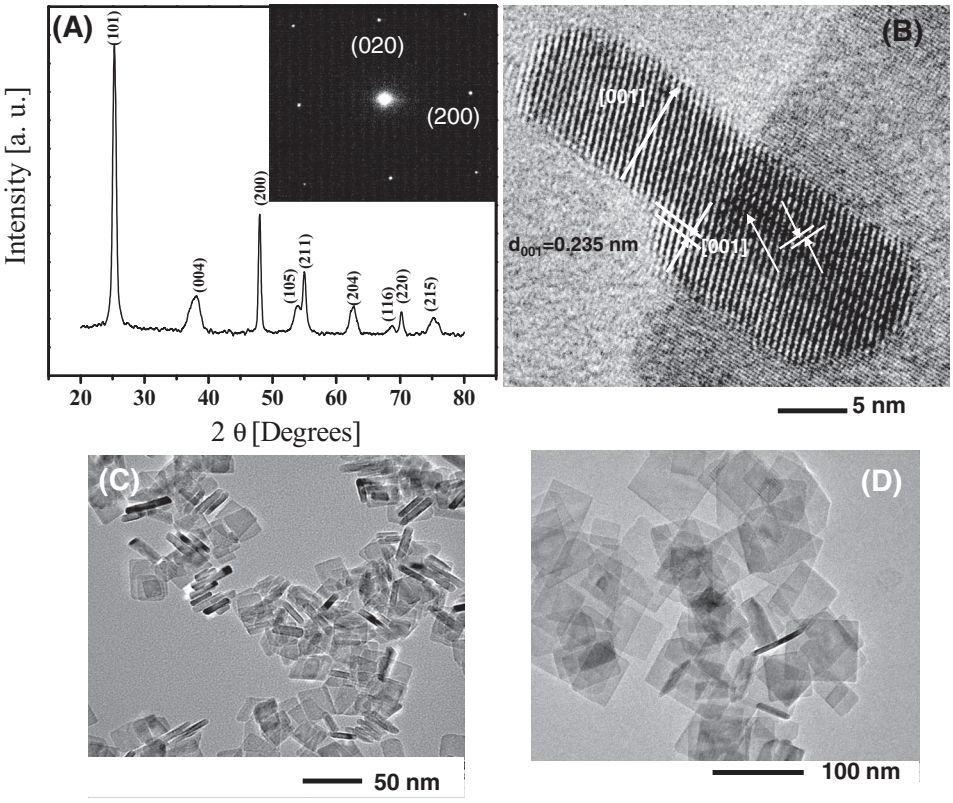

Figure 1. (A) XRD pattern and (B) High-magnification TEM image of an individual TiO_2 nanosheet. (C) Low-magnification TEM image of 30 nm TiO_2 nanosheets synthesized at 180 °C using 10 mL of $Ti(OBu)_4$ and 0.8 mL of HF. (D) Low-magnification TEM image of 80 nm TiO_2 nanosheets synthesized at 200 °C using 10 mL of $Ti(OBu)_4$ and 1.6 mL of HF. Inset of Figure1A: Typical SAED pattern of an individual TiO_2 nanosheet.

(oleic acid) were replaced by mercaptopropionic acid (MPA) during deposition. A gold contact was evaporated on top of the PbS QD film.

Two sizes of PbS QDs were used in this study. The absorption spectra of the PbS QDs are presented in the supporting information (Figure 1S in the SI) and correspond to band gaps (Eg) of 1.38 eV and 1.24 eV.

The operation mechanism of the PbS (QD)/TiO_2 heterojunction solar cell (presented in Figure 2) shows a depletion layer that can extend from the TiO_2 nanosheets film to the QDs film.[13] The local electric field present in the depletion layer is essential in assisting the separation of photogenerated electron hole pairs.

Table 1 summarizes the results obtained for cells made from two sizes of nanosheets (30 and 80 nm) and two sizes of PbS QDs with absorbance of 900 and 1000 nm (corresponding to E_g of 1.38 and 1.24 eV, respectively). In addition, cells using standard TiO_2 NPs with dominantly exposed (101) facets (dyesol paste- DS90) were made for comparison.

We observe that the 30-nm nanosheets give higher short circuit photocurrents than 80-nm nanosheets. The 80-nm nanosheets give a lower efficiency than the TiO_2 NPs. The open circuit voltage (V_{oc}) and current density are smaller for the large QDs (*Eg* of 1.24 eV compared to 1.38 eV) resulting in a lower power conversion efficiency. The best performance was achieved using 30-nm sized TiO_2 nanosheets –in in conjunction with PbS QDs having a bandgap of 1.38 eV.

The differences in the power conversion efficiency can be explained by the BET measurements. The 80-nm sized nanosheets have the lowest surface area of 72 m^2/g while the 30-nm sized nanosheets have the highest surface area of 122 m^2/g. The 18-nm NPs have a specific surface area of 75 m^2/g. It is surprising that the smaller nanosheets produce a substantially higher photocurrent than the larger ones. Possibly, the photo-induced charge separation at the interface between the PbS-QD layer and TiO_2 nanosheets is enhanced by an increase in the

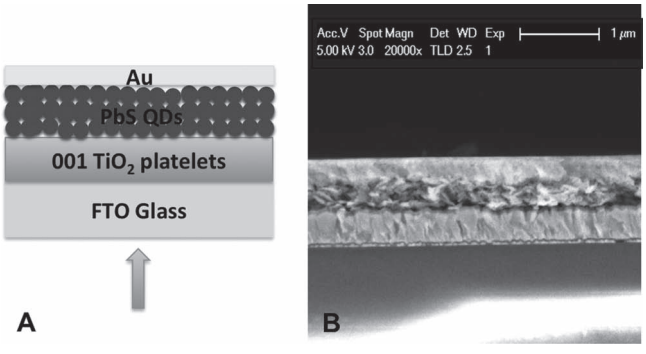

Figure 2. (A) The architecture of the PbS(QD)/nanosheets TiO_2 heterojunction photovoltaic device, the light is incident through the glass. (B) Cross sectional HR-SEM of the photovoltaic device. It shows that the PbS QDs form a nanocrystalline layer on top of the TiO_2 film very few QDs penetrate into the nanosheets network of the TiO_2 film.

Table 1. Comparison of the *J–V* characteristics made from different sizes of TiO_2 nanosheets and PbS QDs.

TiO_2 Sample	BET [m^2/g]	QD *Eg* [eV]	V_{oc} [V]	J_{sc} [mA cm^{-2}]	FF	$\eta^{a)}$ [%]
TiO_2 18-nm NPs (DS90)	75	1.38	0.543	16.3	0.41	4.04
TiO_2 nanosheets 30 nm size	122	1.38	0.545	20.5	0.38	4.73
TiO_2 nanosheets 30 nm size	122	1.24	0.488	16.6	0.46	4.17
TiO_2 nanosheets 80 nm size	72	1.38	0.561	10.6	0.45	3.16
TiO_2 nanosheets 80 nm size	72	1.24	0.46	9.41	0.53	2.73

[a)] The power conversion efficiencies were measured by using a solar simulator whose power output adjusted to match 0.9 full sunlight intensity (90 mW/cm^2) by using a reference Si photodiode.

number of contact points between the two nanomaterials upon reducing the platelet size. The better photovoltaic performance of the nanosheets compared to nanoparticles may be attributed to the higher ionic charge of the exposed (001) compared to the (101) facets strengthening the attachment of the QDs to the TiO_2 surface.[27]

The data in Table 1 also reveal that the PbS particles with a 1.24 eV *Eg* yield a lower open circuit voltage than those with *Eg* of 1.38 eV. This can be explained by the quantum size effect which would reduce the built-in junction potential for the smaller PbS particles at equal doping levels. As a result, the V_{oc} increases by increasing the QD *Eg*.

Figure 3A presents the photovoltaic results obtained for all samples include: standard TiO_2 NPs, two sizes of TiO_2 nanosheets with exposed (001) facets using PbS QDs with *Eg* of 1.38 and 1.24 eV. We obtain the best performance with quantum dots having a diameter of about 3.2 nm. (1st excitonic peak at 900nm, E_g = 1.38 eV) These PbS quantum dots produce a V_{oc} of 0.545 V, a J_{sc} of 20.5 mA cm^{-2} and a fill factor of 38% corresponding to a PCE of 4.7% under 0.9 sun intensity.

The incident photon to current conversion efficiency (IPCE) specifies the ratio of extracted electrons to incident photons at a given wavelength. The IPCE spectra (Figure 3B) are plotted as a function of wavelength of the light. The solid state QDs cell shows a good response from the visible through the near infra-red (NIR), the IPCE spectrum using the TiO_2 nanosheets is reaching its maximum of 100% at 420 nm (rectangles) while the IPCE spectrum using the TiO_2 NPs is reaching its maximum of 90% at 400 nm. Photons of these wavelengths are converted most efficiently as they are absorbed by PbS particles located close to the TiO_2 interface. The excitonic peak of the PbS QDs is observed at 940nm for both cells corresponding to IPCE of 30% and 15.5% for the nanosheets and the NPs respectively. Those peaks are slightly red shifted compared to the first excitonic peak of the QDs (solid curve in Figure 3B) as a result

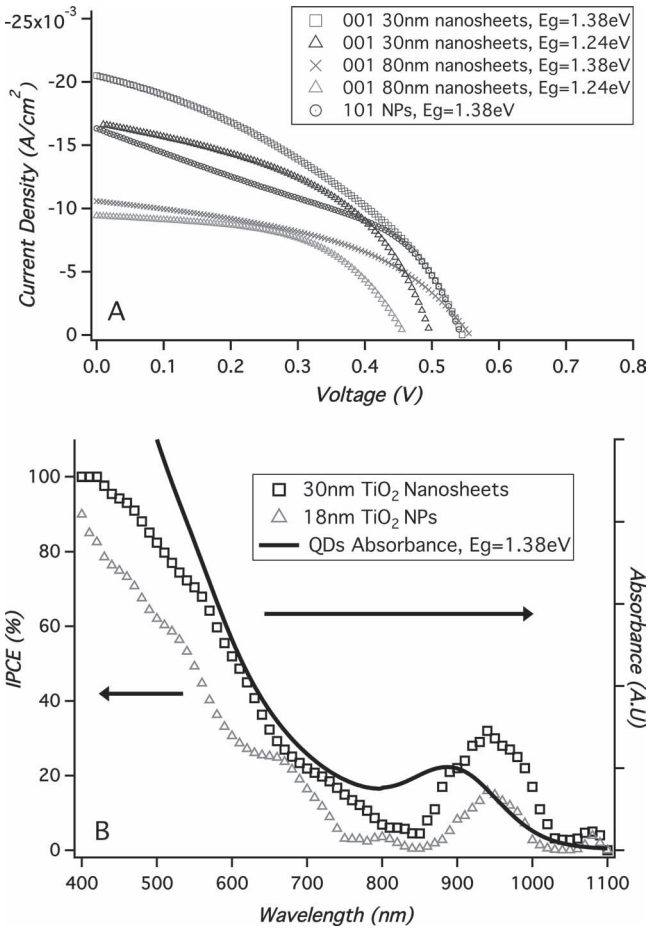

Figure 3. (A) Comparison of the *J–V* characteristics for the solid state PbS QD device. A mask with aperture area of 0.12 cm^2 was placed over the device. (B) IPCE spectra of the PbS QD/TiO_2 heterojunction solar cell. The rectangles show the heterojunction solar cell using (001) 30 nm nanosheets which produced the highest power conversion efficiency; The triangles show the heterojunction solar cell using TiO_2 NPs; and the solid curve shows the absorbance spectrum of the PbS QDs with Eg of 1.38eV.

of film formation. Integration of the IPCE spectrum over the AM1.5 solar emission yields a photocurrent density of 18.2 and 13.7 mA/cm^2 for the nanosheets and the NPs, respectively, which is in reasonable agreement with the measured values. We can attribute the close to 100% IPCE to the efficient attachment of the QDs to the (001) facets of the TiO_2 nanosheets, resulting in near-quantitative conversion of 400–420 nm photons into electric current. As a result of the high IPCE values the absorbed photon–to–current efficiency (APCE) was calculated by measuring the light harvesting efficiency. The APCE exceeds 100% which suggests of multiple exciton generation in the PbS QD/TiO_2 heterojunction solar cell (see Figure 2S in SI).

Anatase TiO_2 nanosheets with 30-nm and 80-nm size and with dominant (001) facets were synthesized and employed in PbS QD/TiO_2 heterojunction solar cell. The best photovoltaic performance was achieved using 30-nm TiO_2 nanosheets with PbS QDs having Eg of 1.38eV. The photovoltaic parameters give a J_{sc} of 20.5 mA/cm^2, a V_{oc} of 0.545V, a FF of 0.38 corresponding

to a solar to electric power conversion efficiency (η) of 4.73% under 0.9 light intensity. The higher surface area related to the small nanosheets and the high reactivity of the (001) facets contribute to the better performance of the PbS QD/TiO_2 heterojunction solar cell compared to standard TiO_2 NPs.

Experimental Section

Synthesis and Purification of TiO_2 Nanosheets: The synthesis of the nanosheets was followed a typical experimental procedure.[28] Ti(OBu)4 (10 mL, 98%) and hydrofluoric acid (0.8 mL, 47%) solution mixed in a 150 mL dried Teflon autoclave which was kept at 180 °C for 24 h to yield the small nanosheets. The synthesis of the big nanosheets followed the same procedure as that for the small nanosheets except using 1.6 mL of hydrofluoric acid and the Teflon autoclave was kept at 200 °C for 24h. After the reaction was cooled to room temperature, the white powder was separated by high-speed centrifugation and washed with ethanol followed by distilled water for several times. *Caution:* Hydrofluoric acid is extremely corrosive and a contact poison, it should be handled with extreme care! Hydrofluoric acid solution is stored in Teflon containers in use.

Nanosheets Characterization: The morphologies of TiO_2 nanosheets were examined by transmission electron microscopy (TEM; JEM 2010F, JEOL, Japan) and selected area electron diffraction (SAED) operated at 200 kV with a drop of TiO_2 nanosheet suspension in methanol mounted onto a carbon-coated 200 mesh Cu grid. The crystal structure of TiO_2 nanosheets was investigated by an X-ray diffraction technique (XRD-6000, Shimadzu, Japan) using Ni-filtered Cu Kα line ($\lambda = 0.15418$ nm) at a scanning rate of 2° min^{-1} in 2θ ranging from 20° to 80°. The Brunauer–Emmett–Teller (BET) surface area of TiO_2 nanosheets was characterized using N_2 adsorption a t–196 °C on a Multi-Station High Speed Gas Sorption Analyzer (Quantachrome, NOVA 3000) in the relative pressure range (P/P_0) of 0.05–0.35.

Methods and Device Fabrication: Colloidal PbS QDs were synthesized according to the method reported by Hines et al.[29] As-prepared PbS QDs were capped with oleic acid (OA). The first excitonic absorption bands of QDs were tuned by controlling reaction temperatures and concentrations of the precursors. The PbS QDs were stored in nitrogen glove box.

During device fabrication, a thin blocking layer of compact TiO_2 was first deposited by spray pyrolysis onto a pre-cleaned FTO glass substrate using a solution of titanium diisopropoxide bis(acetylacetonate) in ethanol as precursor. Subsequently, a nanosheet TiO_2 layer was deposited by spin coating (4000 rpm for 10 sec) from a dilute aqueous solution containing a mixture of TiO_2 nanosheets and ethanol (volume ratio of 1:3). This results in a nanosheet titania film with 300 ± 50 nm thickness. The procedure for the deposition of the PbS QD film is similar to the one reported by Sargent et al.[13] with modifications. The PbS QDs were subsequently deposited layer by layer on the porous TiO_2 film by spin coating a 50 mg mL^{-1} solution in octane. Each layer was cast at a spinning rate of 2500 rpm applied for 10 s and treated thereafter briefly with a solution of 10% 3-mercaptopropionic acid (MPA, ≥99.0% from Sigma Aldrich) in methanol using again 2500 rpm rotational speed for 10 s. This treatment displaced the oleate ligand completely and rendered the QD insoluble, which allowed thin films of 300 nm thicknesses to be created using 12 successive deposition cycles. Each layer was rinsed with anhydrous methanol (purchased from Sigma Aldrich) to remove excess of MPA and PbS QDs. Finally, a gold back contact of ~100 nm thickness was deposited by evaporation through a shadow mask. The device was then completed by encapsulation in Argon atmosphere. The encapsulation of the device was made by placing 2-mm glass on top of the active area of the device using a frame of hot melt Surlyn (25 µm thick) as a sealant and spacer. After encapsulation, the device was stable in ambient air.

The cross section of the device was measured by high-resolution scanning electron microscopy (HR-SEM) FEI XL30 SFEG, using 5 kV with magnification of 20KX.

Photovoltaic Characterization: Photovoltaic measurements employed an AM 1.5 solar simulator equipped with a 450W xenon lamp (Model No. 81172, Oriel). Its power output was adjusted to match AM 1.5 global sunlight (100 mW cm^{-2}) by using a reference Si photodiode equipped with an IR-cutoff filter (KG-3, Schott) in order to reduce the mismatch between the simulated light and AM 1.5 (in the region of 350–750 nm) to less than 2% with measurements verified at two PV calibration laboratories [ISE (Germany), NREL (USA)]. *I–V* curves were obtained by applying an external bias to the cell and measuring the generated photocurrent with a Keithley model 2400 digital source meter. The voltage step and delay time of photocurrent were 10 mV and 40 ms, respectively. A similar data acquisition system was used to determine the monochromatic incident photon- to-electric current conversion efficiency. Under full computer control, light from a 300 W xenon lamp (ILC Technology, U.S.A.) was focused through a Gemini-180 double monochromator (Jobin Yvon Ltd., U.K.) onto the photovoltaic cell under test. The monochromator was incremented through the visible spectrum to generate the IPCE (λ) as defined by IPCE (λ)) = $1240(J_{sc}/\lambda\phi)$, where λ is the wavelength, J_{sc} is the short-circuit photocurrent density (mA cm^{-2}), and ϕ is the incident radiative flux (mW cm^{-2}). Photovoltaic performance was measured by using a metal mask with an aperture area of 0.12 cm^2.

Supporting Information

Supporting Information is available from the Wiley Online Library or from the author.

Acknowledgements

L.E. acknowledges the Marie Curie Actions—Intra-European Fellowships (FP7-PEOPLE-2009-IEF) under grant agreement n° 252228, project "Excitonic Solar Cell". This research was also funded by the European Community's Seventh Framework Programme (FP7/2007-2013) under grant agreement n° 227057, Project "INNOVASOL". B. Liu thanks Singapore National Research Foundation (R279-000-276-272) for financial support. M.G. thanks the European Research Council for financial support under the Advanced Research Grant "Mesolight."

Received: November 24, 2011
Revised: January 23, 2012

[1] W. U. Huynh, J. J. Dittmer, A. P. Alivisatos, *Science* **2002**, *295*, 2425.
[2] I. Gur, N. A. Fromer, M. I Geier, A. P Alivisatos, *Science* **2005**, *310*, 462.
[3] W. J. E. Beek, M. M Wienk, R. A. J. Janssen, *Adv. Func. Mater.* **2006**, *16*, 1112.
[4] J. M. Luther, M. Law, M. C. Beard, Q. Song, M. O. Reese, R. J. Ellingson, A. J. Nozik, *Nano Lett.* **2008**, *8*, 3488.
[5] W. Ma, J. M. Luther, H. Zheng, Y. Wu, A. P. Alivisatos, *Nano lett.* **2009**, *9*, 1699.
[6] R. Plass, S. Pelet, J. Krueger, M. Grätzel, U. Bach, *J. Phys. Chem. B* **2002**, *106*, 7578.
[7] B. Sun, A. T. Findikoglu, M. Sykora, D. J. Werder, V. I. Klimov, *Nano Lett.* **2009**, *9*, 1235.
[8] J. M. Luther, M. Law, Q. Song, C. L. Perkins, M. C. Beard, A. J. Nozik, *ACS Nano* **2008**, *2*, 271.
[9] S. Zhang, P. W. Cyr, S. A. McDonald, G. Konstantatos, E. H. Sargent, *Appl. Phys. Lett.* **2005**, *87*, 233101.
[10] B.-R. Hyun, Y.-W. Zhong, A. C. Bartnik, L. Sun, H. D. Abruña, F. W. Wise, J. D. Goodreau, J. R. Matthews, T. M. Leslie, F. Borrelli, *ACS Nano* **2008**, *2*, 2206.

[11] D. Ratan, T. Jiang, D. A. Barkhouse, W. Xihua, G. P.-A. Andras, B. Lukasz, L. Larissa, E. H. Sargent, *J. Amer. Chem. Soc.* **2010**, *132*, 5952.
[12] J. M. Luther, J. Gao, M. T. Lloyd, O. E. Semonin, M. C. Beard, A. J. Nozik, *Adv. Mater.* **2010**, *22*, 3704.
[13] A. G. Pattantyus-Abraham, I. J. Kramer, A. R. Barkhouse, X. Wang, G. Konstantatos, R. Debnath, L. Levina, I. Raabe, M. K. Nazeeruddin, M. Gratzel, E. H. Sargent, *ACS Nano* **2010**, *4*(6), 3374.
[14] H. Liu, J. Tang, I. J. Kramer, R. Debnath, G. I. Koleilat, X. Wang, A. Fisher, R. Li, L. Brzozowski, L. Levina, E. H. Sargent, *Adv. Mater.* **2011**, *23*, 3832.
[15] J. Gao, J. M. Luther, O. E. Semonin, R. J. Ellingson, A. J. Nozik, M. C. Beard, *Nano Lett.* **2011**, *11*, 1002.
[16] J. Gao, C. L. Perkins, J. M. Luther, M. C. Hanna, H. Y. Chen, O. E. Semonin, A. J. Nozik, R. J. Ellingson, M. C. Beard, *Nano Lett.* **2011**, *11*, 3263.
[17] D. A. R. Barkhouse, R. Debnath, I. J. Kramer, D. Zhitomirsky, A. G. Pattantyus-Abraham, L. Levina, L. Etgar, M. Grätzel, Edward H. Sargent, *Adv. Mater.* **2011**, *23*, 3134.
[18] X. Wang, G. I. Koleilat, J. Tang, H. Liu, I. J. Kramer, R. Debnath, L. Brzozowski, D. A. R. Barkhouse, L. Levina, S. Hoogland, E. H. Sargent, *Nat. Photonics* **2011**, *5*, 480.
[19] K. S. Leschikies, T. J. Beatty, M. S. Kang, D. J. Norris, E. S. Aydil, *ACS Nano* **2009**, *3*, 3638.
[20] F. W. Wise, *Acc. Chem. Res.* **2000**, *33*, 773.
[21] J. B. Sambur, T. Novet, B. A. Parkinson, *Science* **2010**, *330*, 63.
[22] C. M. Evans, L. Guo, J. J. Peterson, S. Maccagnano-Zacher, T. D. Krauss, *Nano Lett.* **2008**, *8*, 2896.
[23] M. V. Kovalenko, D. V. Talapin, M. A. Loi, F. Cordella, G. Hesser, M. I. Bodnarchuk, W. Heiss, *Angew. Chem. Int. Ed.* **2008**, *47*, 3029.
[24] R. D. Schaller, V. I. Klimov, *Phys. Rev. Lett.* **2004**. *92*, 186601.
[25] M. Lazzeri, A. Vittadini, A. Selloni, *Phys Rev. B* **2001**, 63.
[26] H. G. Yang, C. H. Sun, S. Z. Qiao, J. Zou, G. Liu, S. C. Smith, H. M. Cheng, G. Q. Lu, *Nat. Lett.* **2008**, *453*, 638.
[27] L. Kavan, M. Graetzel, S. E. Gilbert, C. Klemenz, H. J. Scheel, *J. Am. Chem. Soc.* **1996**, *118*, 6716.
[28] X. Han, Q. Kuang, M. Jin, Z. Xie, L. Zheng, *J. Am. Chem. Soc.* **2009**, *131*, 3152.
[29] M. A. Hines, G. D. Scholes, *Adv. Mater* **2003**, *15*, 1844.